Earth and Planetary Science Letters 567 (2021) 117009

Contents lists available at ScienceDirect

Earth and Planetary Science Letters

www.elsevier.com/locate/epsl

Rapid erosion of the central Transantarctic Mountains at the Eocene-Oligocene transition: Evidence from skewed (U-Th)/He date distributions near Beardmore Glacier

John He [a,*], Stuart N. Thomson [a], Peter W. Reiners [a], Sidney R. Hemming [b], Kathy J. Licht [c]

[a] Department of Geosciences, University of Arizona, Tucson, AZ 85721, USA
[b] Lamont-Doherty Earth Observatory of Columbia University, Palisades, NY 10964, USA
[c] Department of Earth Sciences, Indiana University Purdue University Indianapolis, Indianapolis, IN 46202, USA

ARTICLE INFO

Article history:
Received 15 January 2021
Received in revised form 20 April 2021
Accepted 12 May 2021
Available online 27 May 2021
Editor: A. Webb

Keywords:
apatite helium thermochronology
overdispersion
East Antarctic ice sheet
subglacial landscape
glacial erosion

ABSTRACT

Apatite (U-Th)/He thermochronology has the potential to reconstruct records of erosional exhumation that are critical to understanding interactions between climate, tectonics, and the cryosphere at high latitudes on million-year timescales. However this approach is often hindered by the problem of intrasample single-grain date dispersion. Here we present an extensive new apatite (U-Th)/He dataset (n = 361) from the central Transantarctic Mountains of East Antarctica between 160°E to 170°W and 84 to 86°S, and show that apparently uninterpretable data in most samples are a reflection of inadequate sampling of skewed date distributions. We outline a workflow for interpreting such dispersed data and demonstrate that geologically meaningful age interpretations are possible in the case of rapidly cooled samples, despite the wide array of potential causes for date dispersion. We show that for samples and compilations with a large number of single-grain analyses (n > ~25), the youngest probability distribution peak represents the most likely time of fast cooling through the apatite (U-Th)/He closure temperature. When fewer grains are analyzed, the youngest peak is represented best by the minimum date or first quartile date, depending on sample size. Using this workflow, we show that since the latest Eocene, up to 8.8 km of exhumation occurred to incise the deepest point of the Beardmore Glacier trough. Rapid incision began at c. 37-34 Ma (at the latest by 34±3 Ma), coinciding with or slightly preceding the initiation of Antarctic glaciation at the Eocene-Oligocene transition, and contributed to at least 2.6 km of exhumation within the first 3-6 million years, at an apparent exhumation rate of no less than 0.4 mm/a.
© 2021 Elsevier B.V. All rights reserved.

1. Introduction

The problem of large intrasample dispersion of single-grain dates has long vexed apatite (U-Th)/He thermochronology (Fitzgerald et al., 2006; Vermeesch, 2008; Gautheron et al., 2009; Flowers and Kelley, 2011; Peyton et al., 2012; Brown et al., 2013; Flowers et al., 2015; Zeitler et al., 2017; McDannell et al., 2018). Although the technique provides reproducible and useful results in many cases for certain thermal histories and lithologies, for others it yields data far more scattered than can be explained by analytical uncertainty. In some cases, date variation can be correlated with crystal size or parent nuclide concentration (effective uranium concentration, or eU), yielding additional information about a sample's thermal history (e.g. Reiners and Farley, 2001; Flowers et al., 2009). In others, dispersion may arise from a variety of other potential sources including inclusions (Vermeesch et al., 2007), implantation (Spiegel et al., 2009; Gautheron et al., 2012; Murray et al., 2014), eU zonation (Ault and Flowers, 2012; Farley et al., 2011), fragmentation (Brown et al., 2013), systematic measurement uncertainty (Cooperdock et al., 2019), and microstructural defects (Zeitler et al., 2017; McDannell et al., 2018). Yet despite conscientious screening protocols and increasingly sophisticated understanding of the uncertainties of apatite helium dating, a clear answer to the problem of cryptic dispersion remains elusive.

A prime illustration of this conundrum comes from a study by Fitzgerald et al. (2006) in the Transantarctic Mountains of southern Victoria Land. Here apatite fission track data from three date-elevation transects provided robust constraints on the early thermal history, indicating an increase in exhumation starting in early to middle Eocene time. In contrast, apatite He dates showed significant dispersion, providing no clear resolution of the thermal history post-50 Ma, beyond perhaps their interpretation of slow

* Corresponding author.
E-mail address: johnhe@arizona.edu (J. He).

https://doi.org/10.1016/j.epsl.2021.117009
0012-821X/© 2021 Elsevier B.V. All rights reserved.

cooling through the apatite He partial retention zone (PRZ). This dispersion is unfortunate because the low closure temperature of the apatite He system (~45-70 °C for typical crystal sizes, eU, and cooling rates, corresponding to exhumation through depths of ~2-3 km) presents one of the most promising means of accessing the shallowest segment of the time-temperature record relevant to many surface processes (Flowers et al., 2009). A clearer record of the Cenozoic exhumation histories in Antarctica could address many outstanding questions about the interplay of the cryosphere, climate, and erosion (Whitehouse et al., 2019): for example, how ice-sheet dynamics shape the pattern of glacial erosion in Antarctica, and conversely, how mass redistribution and isostatic adjustment control ice-sheet formation and stability (Stern et al., 2005; Siegert, 2008; Gasson et al., 2015).

Here we present an extensive new apatite (U-Th)/He dataset ($n = 361$ single-grain dates) from the central Transantarctic Mountains (TAM), covering an area of ~60,000 km^2, and evaluate it in conjunction with compiled data from existing literature. We demonstrate that for rapidly cooled samples, robust age interpretation is possible despite large data dispersion, even when there is no clear correlation between date and eU or grain size. Taking into account the effect of glacial incision and topographic warping of isotherms, we constrain the time of onset of rapid exhumation, estimate the amount of exhumation that occurred since late Eocene, and discuss possible correlations of the exhumation record with tectonics and/or climatic and cryospheric transitions.

2. Cryosphere and erosion: apatite helium data in East Antarctica

Increasingly precise paleoclimate records document the uneven transition from greenhouse to icehouse conditions in the Cenozoic (Fig. 1a). For the first 10-15 Ma after the Eocene-Oligocene transition, changes in the East Antarctic Ice Sheet (EAIS) were recorded in prominent glaciomarine cycles of expansion and retreat (Zachos et al., 2008; Liu et al., 2009; Galeotti et al., 2016). During this time of dynamic ice-sheet conditions, particularly in late Oligocene and mid-Miocene, minima in oxygen isotope values imply several warm intervals of low or no ice volume (Liebrand et al., 2017). After the mid-Miocene, oxygen isotope values steadily climbed, indicating a more frigid climate closer to that of Antarctica today, where summer temperatures typically remain below freezing (Wilson et al., 2008).

Climate-cryosphere changes are coupled to Antarctic subglacial landscape evolution. Theory and modern observations suggest that the rate of subglacial erosion is partly a function of basal-melt rates, because subglacial streams can both directly incise into the bedrock and also evacuate subglacial till (Alley et al., 2019). Transitions from temperate to polar thermal regimes thus lead to reduced subglacial erosion and decreased capacity to transport subglacial debris (Koppes et al., 2015; Alley et al., 2019). However, a record of paleotopography in Antarctica is needed to substantiate whether these observations can be extrapolated to geologic timescales, and to better inform numerical modeling of past EAIS evolution in response to climate perturbations.

Previous characterizations of paleotopographic evolution rely largely on assumptions of erosional pathways and processes, and estimates of sediment volume and sedimentation rate inferred from offshore or onshore glacial deposits (Jamieson et al., 2010; Lindeque et al., 2016; Gulick et al., 2017; Paxman et al., 2019; Hochmuth et al., 2020). These lines of evidence provide important, albeit indirect, inferences about bedrock erosion. In particular, correlations of hiatuses and pulses of glaciogenic sedimentation with episodes of icesheet expansion are limited because sediment cores are single-point estimates, which cannot fully capture the spatial and temporal variability of autogenic sedimentary processes (e.g. cyclic or episodic sediment transport and storage), even in major glaciation events (Roberts et al., 2003; Francis et al., 2008).

The Transantarctic Mountains, on the other hand, provide direct, three-dimensional exposures of exhumed, glacially-incised bedrock. However, in most locations in Antarctica, exhumation has been insufficient to expose apatite fission track dates younger than about 45 Ma (Fitzgerald, 1992; Fitzgerald and Stump, 1997; Fitzgerald et al., 2006), leaving apatite He dating as the best tool to provide this missing link. Unfortunately, the problem of cryptic date dispersion outlined by Fitzgerald et al. (2006) has continued to confound later studies throughout much of the TAM: a compilation of all published apatite He data from East Antarctica, along with new samples from this study, reveals the extent of the problem (Fig. 1b). Intrasample date ranges can be tens of millions of years, complicating age interpretation. Though the minimum dates hint at an interpretable date-elevation relationship, no consensus has been reached on the choice of the appropriate summary statistic to represent such dispersed data. This illustrates the key interpretational dilemma: any decision in how to represent data would be arbitrary without knowledge of the underlying date distribution and causes of dispersion.

3. Methods

To obtain a more detailed record of the low-temperature thermal and exhumation history of the central TAM, we analyzed apatite He dates from 67 samples from near the Beardmore Glacier and Shackleton Glacier; most samples were collected within 150 km of TAM front (Fig. 2). Samples were collected during a field campaign in December 2017 (yellow circles), augmented by additional samples provided by the U.S. Polar Rock Repository (PRR; red circles).

The samples used are part of a larger, ongoing thermochronologic study of the central TAM. In this paper, we present the apatite He data and thus the lowest-temperature portion of the thermal history, focusing in particular on two vertical transects ~25 km apart: Barnes Peak (BAR) and Cloudmaker (CMK). The top of the BAR transect is ~800 m higher than the top of CMK, and they are separated by the Kukri Peneplain, a gently dipping Paleozoic erosional surface (Fig. 2b). Cloudmaker samples below the nonconformity are Cambrian granitoids, whereas Barnes Peak samples above the nonconformity are Permian to Jurassic sandstones of the Beacon Supergroup (except BAR-2538B).

All (U-Th)/He analyses were performed at the University of Arizona following routine protocols (Supplementary Methods). Single-grain dates are presented in Supplementary Table 1 and discussed in Section 4; all subsequent steps taken to represent and interpret those dates are presented in Sections 5–6. First, we examine in detail the causes of date variation and dispersion, rule out possible sources of dispersion, and consider the expected probability distributions of dates from a rapidly cooled sample, in order to determine a geologically meaningful age. We then apply this analysis to the new dataset, and evaluate the actual probability distribution of dates from large-n analyses of single samples and from compilations of adjacent-elevation samples from the two transects. Those distributions are used to select the most appropriate statistics to represent the date peak, to make age interpretations, and to constrain the magnitude and rate of exhumation near the Beardmore Glacier. Finally, we consider an elevation-weighted probability distribution of the broader regional dataset in light of those interpretations (Supplementary Methods).

4. Data

Despite our best attempts to screen grains for imperfections, the samples yielded widely dispersed single-grain apatite He dates,

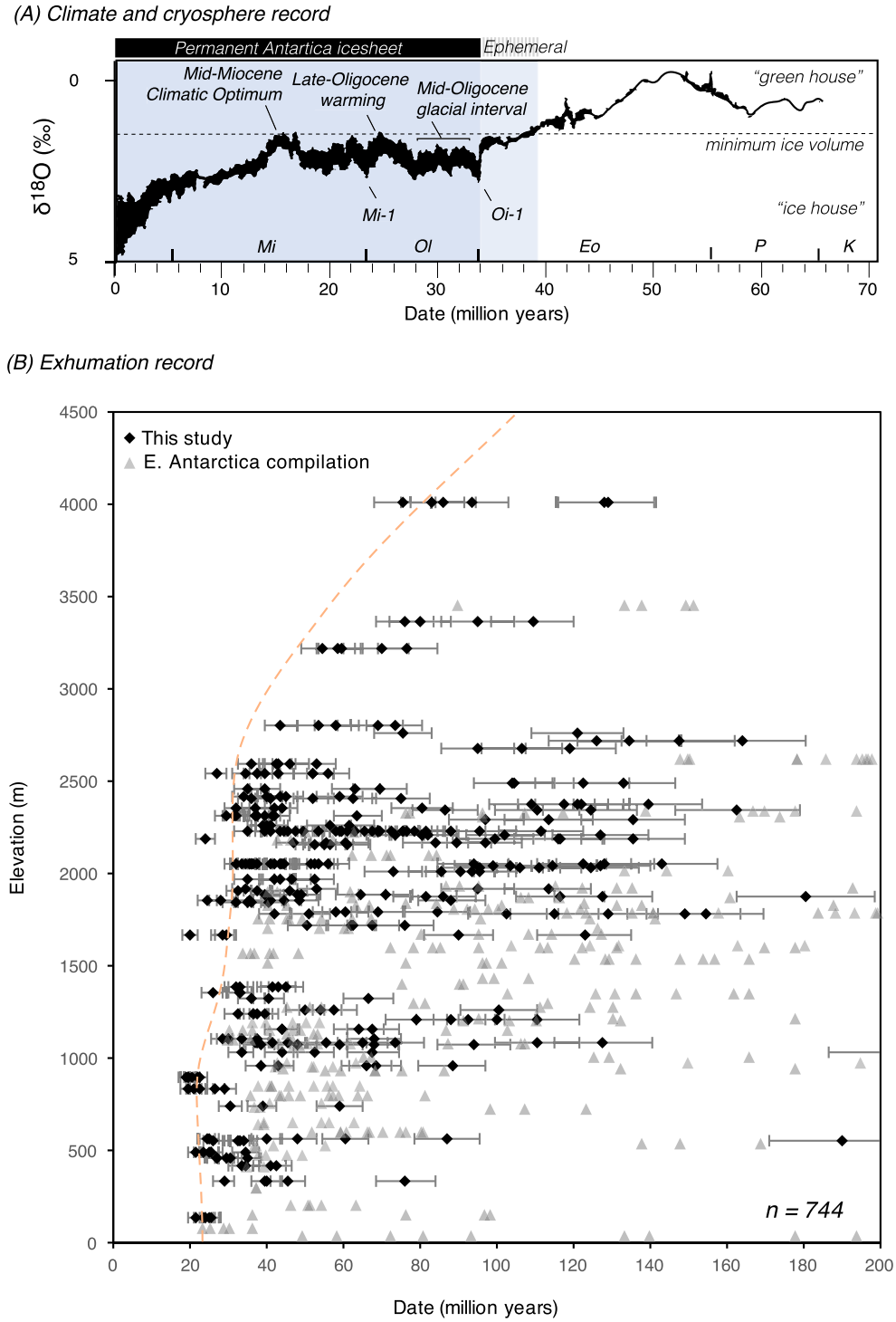

Fig. 1. Comparison of the precision of climate records and the relative imprecision of exhumation records. **(a)** Summary of major Cenozoic climatic transitions based on stacked benthic foraminferal oxygen-isotope records (after Zachos et al., 2008); **(b)** Compilation of apatite (U-Th)/He data from East Antarctica, showing the large scatter of single-grain dates within each sample, at any given elevation or location (See supplement for compiled data and sources; detrital data are not included). As an example, the dashed red line indicates one possible interpretation of a date-elevation trend. However, note that the compilation of data in this figure does not imply that a single cooling history applies to all study areas. One outlier grain (<10 Ma) is excluded. For clarity, error bars are included only for dates from this study. Because analytical uncertainty of individual grains is usually much smaller than natural dispersion in grain dates, we show an estimate of the 95% CI for date error due to zonation variation (see text for discussion). (For interpretation of the colors in the figure(s), the reader is referred to the web version of this article.)

with the oldest date more than double the youngest date in many samples. The large dispersion is difficult to decipher (Fig. 1b, black diamonds; Supplementary Table 1), and the mean dates show no discernable date-elevation trends. A near-vertical line at ~35 Ma arguably marks an approximate minimum trend, between ~1.0 to 2.5 km in elevation. The top three samples of Barnes Peak yield single-grain dates that are all significantly older than the rest of the samples from both transects, defining a break-in-slope in the date-elevation trend that we interpret as the base of a preserved apatite He PRZ (see Section 6.1).

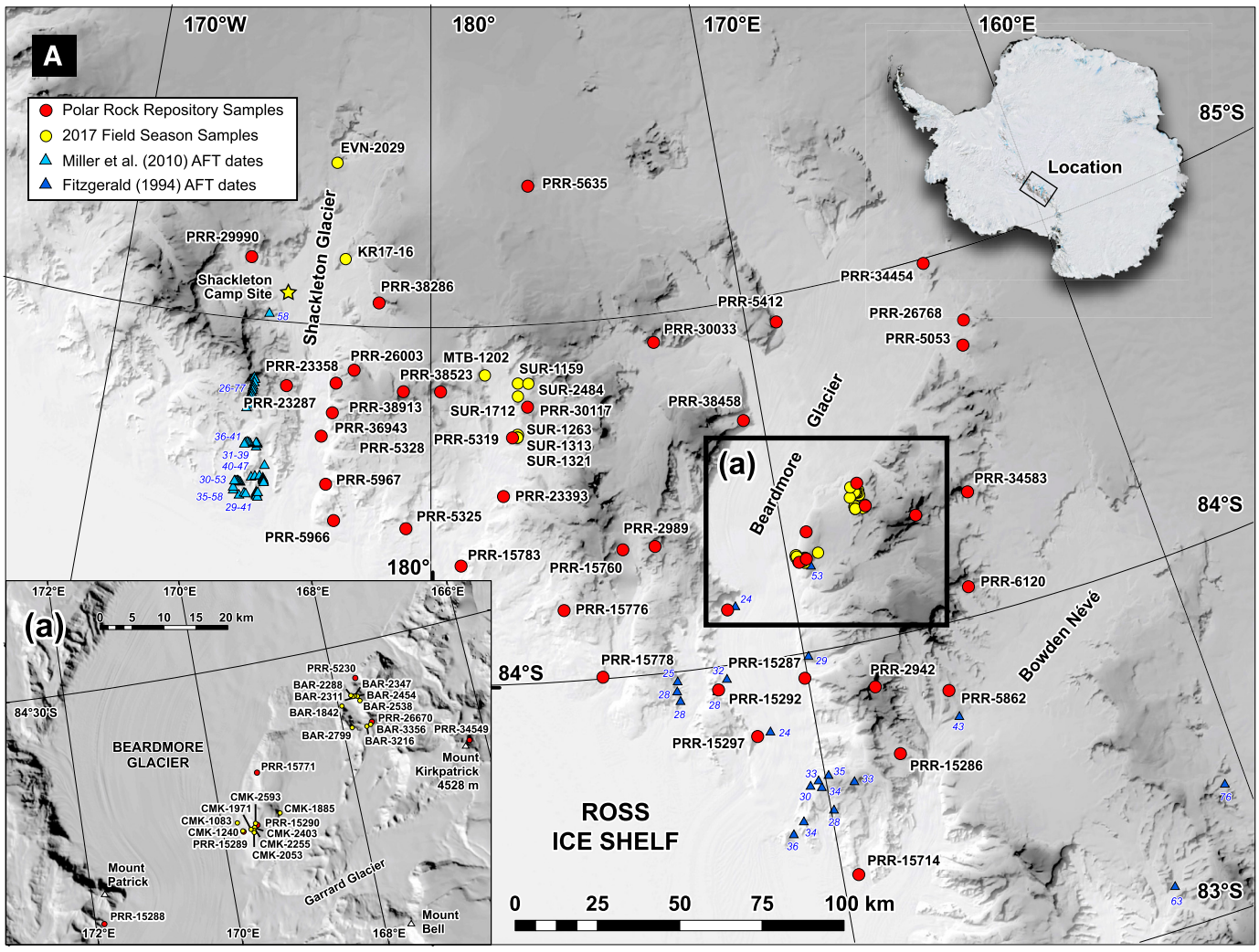

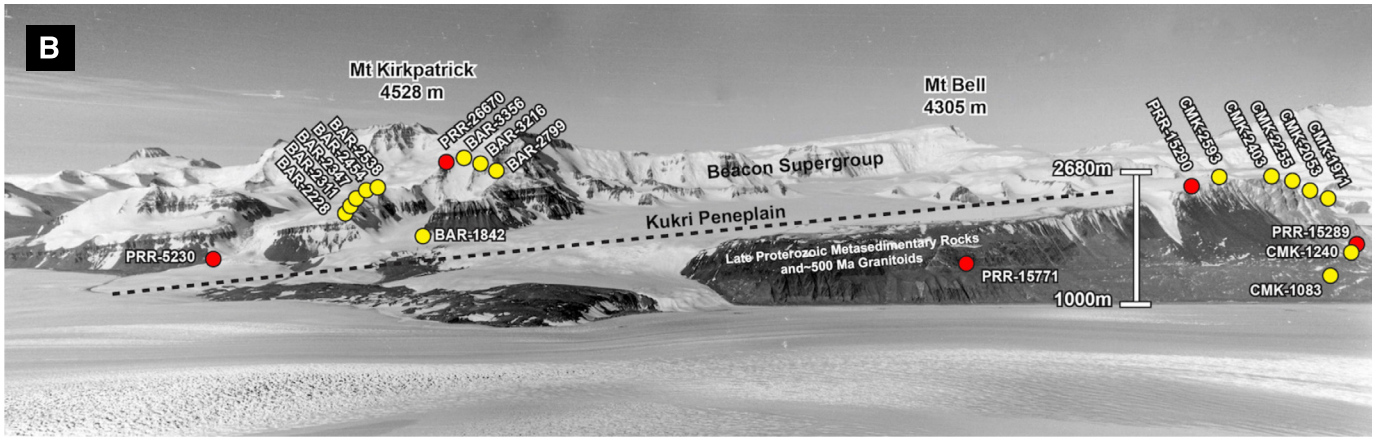

Fig. 2. Sample Locations. **(a)** Map of samples from the field (CMK- Cloudmaker; BAR – Barnes Peak; KR-Kitching Ridge; EVN- Everett Nunatak; MTB- Mt. Bellows) and from the Polar Rock Repository (PRR), and previous thermochronology studies; **(b)** annotated photograph (cropped and edited for clarity) showing the relative locations of vertical transect samples relative to the tilt of the Kukri Peneplain and Beacon supergroup strata. Restoring the dip of the unconformity to horizontal would add ~0.5 km of additional vertical offset between the two transects (assuming regional tilting was associated with post-exhumation rift-flank uplift). Aerial photograph (CA03950312) and DEM courtesy of the Polar Geospatial Center.

Additional field and PRR samples, which provide areal coverage to complement the dense sampling along the transects (Fig. 2), yielded single-grain dates ranging from 20 to 170 Ma, and sample means from 21 to 160 Ma (Supp. Tables). In general, samples near the Beardmore Glacier yielded younger dates than those near the Shackleton Glacier, and the lowest-elevation samples closer to the Ross Sea margin of the TAM have the youngest dates (Supp. Tables).

5. Interpretation of apatite helium dates

To extract geologically meaningful information from the widely dispersed dataset, we systematically considered potential sources of dispersion and error. First, we screened for clear analytical error. We excluded analyses for which grain mass calculated from isotope-dilution measurements of Ca content were less than 25% than expected from that from microscopic dimension measurements, or vice versa (Guenthner et al., 2016). Besides these discrepancies, which could indicate inaccuracy in alpha-ejection corrections related to grain morphology estimates, analytical uncertainty on parent and daughter contents is an unlikely source of significant dispersion (Supp. Fig. 3). We excluded data likely to be imprecise due to very low eU (<5 ppm) or very small grain size (Rs <25 μm). We reviewed grain measurement notes and further excluded those where cracks or staining were suspected or observed, which point to the possible presence of high-eU grain boundary phases (e.g. oxides) (Murray et al., 2014). We also measured trace and rare earth elements (T/REE) for all analyzed grains from the same dissolved aliquots used for U/Th/Sm/Ca measurements (Supp. Tables). However, we found no clear correlations between T/REE geochemistry and sample date or dispersion, except potentially a very weak trend for light rare earth elements (Section 5.1.2).

Next, we considered other sources of dispersion, which are "errors" only insofar as they depart from the ideal assumptions of apatite He dating. These issues have been reviewed at length by other authors (Fitzgerald et al., 2006; Flowers and Kelley, 2011; Brown et al., 2013; Murray et al., 2014). Below, we emphasize observations and conclusions that are relevant to our interpretation of the dispersed dataset.

5.1. Sources of dispersion

5.1.1. Inclusions/inherited/trapped helium

He trapped in fluid inclusions is unlikely to significantly affect apatite He dates unless there is a high density of inclusions, inclusions are very large, or the apatite grains are very young (Farley, 2002). However, trapping of radiogenic He in microvoids may lead to significant date dispersion in older, slowly cooled samples (Zeitler et al., 2017). Another possible source of parentless helium is inclusions of high-eU phases that were not fully dissolved with the rest of the apatite (Farley and Stockli, 2002). However, large inclusions that would significantly affect dates were screened in the picking process, and micro-inclusions are unlikely to contribute enough helium to significantly affect dates (Vermeesch et al., 2007). Previous experiments have shown that use of stronger dissolution procedure to ensure analysis of any unidentified micro-inclusions made no difference in date dispersion (Peyton et al., 2012).

5.1.2. Implantation

High-eU phases adjacent to analyzed grains can eject helium into the grains. Depending on the relative eU of the grain and its neighbor, external sources of helium can cause apparent dates several times the actual date (Spiegel et al., 2009; Gautheron et al., 2012). Though dates from low-eU grains in this dataset do not appear to be systematically more affected by helium implantation, as would be expected (Murray et al., 2014), we cannot exclude the possibility of implantation for any sample (Supp. Fig. 1). To qualitatively evaluate the likelihood of helium implantation from adjacent, high-eU phases, we examined thin sections of representative samples and noted potential cases with unusually high likelihood of implantation, particularly the presence of grain boundary phases/coatings. In most samples, we observed some clustering of accessory minerals (preferential nucleation in igneous samples, e.g. inclusions in biotite, and mechanical separation by density or grain size in sedimentary samples) (Supp. Fig. 2).

We note a possible, weak trend where the oldest grains (normalized to the sample minimum) tend to have low light rare earth element (LREE) concentration, but not all grains low in LREE yielded old dates (Supp. Fig. 4). One interpretation is that hydrothermal or other metasomatic alteration leeched LREE, which was re-precipitated as high-LREE, high-eU grain boundary phases (e.g. monazite) (Harlov, 2015). Because re-precipitated grain boundary phases are generally removed during mineral separation, apatite grains once surrounded by such phases would yield older dates (Murray et al., 2014). Thus, low LREE may indicate increased probability of He implantation, leading to a greater variance in dates. In any case, this trend was not strong enough to warrant the exclusion of any sample, and there is no way to exclude individual dates based simply on low LREE.

5.1.3. Parent zonation and alpha-ejection (F_T) correction errors

Helium loss due to alpha-ejection is corrected using well-understood methods based on the geometry of each analyzed grain (Farley and Stockli, 2002), assuming ideal crystal geometry and homogenous distribution of parent nuclides. Uncertainties arise due to departures from these assumptions. Errors related to geometric approximations are usually only <2% (Cooperdock et al., 2019). Errors due to the use of an unzoned F_T correction for zoned grains lead to older or younger dates depending on the relative eU and thicknesses of the rims (Farley et al., 2011). However, though zonation is common, Ault and Flowers (2012) found in a survey of natural apatite that the difference in eU between core and rim is usually less than a factor of three. Like ours, their study sampled a mix of rock types and a range of grain sizes ($R_s \approx$ 30-140 um). Assuming the distribution of zonation magnitude from that study is representative of most apatite grains, we approximate that for more than 95% of apatite grains, the use of naïve unzoned F_T corrections (despite the presence of zonation) only introduces additional uncertainty of at most 9.3% and 8.5%, for rim-enriched and rim-depleted crystals, respectively. This is consistent with other studies that found <9% additional uncertainty in the most extreme cases (Farley et al., 2011).

To minimize the possibility of misinterpretation from the use of unzoned F_T-correction, we qualitatively assessed the patterns of zonation in each sample, using fission track mounts or induced fission tracks in muscovite detectors (Flowers and Kelley, 2011). While we did not acquire zonation data for each grain analyzed, we observed no significant, systematic patterns of zonation that would bias the apparent date distribution in any given sample (Farley et al., 2011; Ault and Flowers, 2012), with three exceptions noted with asterisks in the date-elevation plot (Supp. Fig. 1). Because these observations relate to the overall sample, and not single-grain analyses, they inform our interpretation of the date distribution of each sample but we do not use them to exclude data.

Dispersion also arises from the application of F_T correction to fragmented grains. Without correction, fragment dates can vary by up to 7% for rapidly cooled samples (Brown et al., 2013). Nevertheless, the application of an adjusted F_T correction to fragments consistently approximates the F_T-corrected date of an unbroken grain within <1% (Supp. Fig. 7).

5.1.4. Diffusive helium loss

Helium diffusion in apatite follows the Arrhenius relationship in accordance with thermally activated volume diffusion, where diffusivity is extrapolated from laboratory measurements of He from step-heated samples, and the diffusion domain is taken to be the crystal size (Farley, 2000). However, grains from the same hand sample (that experienced the same thermal history) may have experienced different extents of He loss due to (i) variable radiation

damage, or possibly differing concentrations or types of crystallographic defects; (ii) differing diffusion domain/crystal size, or (iii) differing zonation effects on diffusive loss.

(i) Most radiation damage in apatite is caused by displacement of atoms by energetic alpha decay, which increases He retentivity (Shuster et al., 2006; Flowers et al., 2009; Gautheron et al., 2009). For slowly cooled samples, this would lead to systematic date-eU correlations, which were not found in the data with one possible exception (Supp. Fig. 5a). Furthermore, zircon He data from till and sedimentary TAM samples indicate that the rocks have been heated to at least ~180 °C, associated with widespread Ferrar magmatism at c. 180 Ma (Welke et al., 2016), which would have annealed any older radiation damage and alpha-induced vacancy defects, limiting the accumulation of radiation damage to post-180 Ma.

As with radiation damage, grains with microstructural defects are thought to have lower diffusivity, effectively higher closure temperature, and thus older dates relative to an otherwise identical grain without such defects. Recent developments in continuous ramped heating (CRH) could potentially improve assessment of data quality and allow screening of anomalous diffusive behavior (McDannell et al., 2018; Idleman et al., 2018; Guo et al., 2019), but this requires continuous measurement of He as temperature is linearly increased until total gas release, which was not implemented in our analyses.

(ii) For certain cooling histories, crystal size can affect retentivity, where larger grains retain more helium in the PRZ, leading to older dates (Reiners and Farley, 2001). However, we observed no systematic date-size relationship for either individual samples or the entire dataset overall (Supp. Fig. 5b). An additional consideration is that if cooling rates through the PRZ were slow, diffusion domains smaller than the actual grain would lead to younger dates, due to more efficient diffusive pathways than volume diffusion. We consider this unlikely, because we exclude grains with visible cracks and other defects from selection for analysis.

(iii) Variable helium concentration profiles due to alpha ejection or extreme parent nuclide zonation can also affect diffusion (Meesters and Dunai, 2002; Farley et al., 2011; Gautheron et al., 2012). Lower helium concentration along rims (e.g. due to alpha ejection) limits diffusive loss, but higher rim concentration (due to extreme eU zonation) enhances it. In the latter case, the greater diffusive loss in addition to greater alpha ejection exacerbates the error arising from the use of unzoned F_T corrections, because they correct for alpha-ejection but not diffusion.

5.2. Expected skew of apparent dates

To summarize Section 5.1, for rapidly cooled samples where dispersion caused by variable eU, grain size, fragmentation, grain chemistry, and zoning are minimized, the largest and most probable sources of anomalous apatite He dates (parentless helium, helium trapping, damage- or defect-modified diffusivity) almost all cause the dates to be older. Uncertainties related to estimation of the alpha-ejection correction would generally be expected to be symmetrically distributed and relatively small (Cooperdock et al., 2019; Supp. Fig. 7). The same is true for parent nuclide zonation, unless most of the grains were affected by a far more extreme and systematic type of zonation than typically seen in apatite, and this is even more unlikely given the range of detrital and magmatic sources of these apatite grains. The only factors that could lead to younger dates are anomalously low He retentivity (i.e., smaller diffusion domain than the grain size, anomalous diffusivity), or systematically under-corrected alpha-ejection effects, either because of morphology or extreme and systematic zonation (especially narrow, high-eU rims), neither of which are supported by our observations during picking and in fission track mounts.

Given the range of potential uncertainty, various protocols have been suggested to deal with overdispersed data (Fitzgerald et al., 2006; Vermeesch, 2008, 2010; Brown et al., 2013), but none have definitively resolved the problem. Fig. 3A shows a date-elevation plot of Cloudmaker and Barnes Peak samples, depicting some of the choices that could be made in displaying and interpreting data, including the minimum, mean of youngest two dates, median, and arithmetic mean. Other ways of representing the data not depicted include the central age or geometric mean (Vermeesch, 2010), and the weighted mean with exclusions based on the Chauvenet criterion (Fitzgerald et al., 2006), which are generally close to but slightly lower than the arithmetic mean.

For samples that have rapidly cooled and show no date-eU or date-size variation, the discussion of uncertainty sources above would support the choice of summary statistics biased towards younger dates as the best representation of the true time of cooling through the apatite He closure temperature. However, many have argued that representation of intrasample data should be unbiased against either younger or older grains. For example, Vermeesch (2010) proposed adopting the central age as a robust, unbiased alternative to the arithmetic mean, both of which are measures of central tendency that explicitly assume unskewed normal distributions. Peyton et al. (2012) suggested that weighted means may be inappropriate because larger absolute analytical uncertainty on older dates bias the weighted means towards younger dates. Such preference for unbiased estimates also finds support in studies that have shown symmetrically distributed dates in some samples (e.g. Cooperdock et al., 2019). Thus, the mere expectation that the combination of uncertainty sources should lead to a skewed distribution of dates does not, by itself, justify the use of minimum dates.

To gain a better understanding of the date dispersion, we can consider these data in concentration-production or abundance-production plots, proposed by Vermeesch (2008), to screen for excess or parentless helium. A minimum envelope clearly defines a consistent isochron running through the origin (Fig. 4), supporting the expectation, as discussed above, that excess He is likely the dominant cause of dispersion and that bias to younger dates (e.g. eU-enriched rims, excess diffusive loss) would be limited. However, without knowledge of what sources of uncertainty are dominant, the selection of different pools of the youngest grains remains a matter of user judgment that could alter the isochron fit, and therefore age interpretation (although the inclusion or exclusion of one or two grains generally does not significantly affect the line fit).

These examples show that the appropriate choice of data representation remains an open question. The wide range of proposed solutions to represent or interpret overdispersion, in the absence of date-eU or date-size variation, raises the possibility that the fundamental problem is not scatter or overdispersion itself, but rather that the underlying nature of the distribution is unknown and uncertainties are not fully accounted for. If a sample's grain dates are normally distributed, the mean remains useful and interpretable even if the variance is large. But if the sample is skewed, with a young peak and long tail, then the mean is misleading even if there is low variance. Any choice of a summary statistic to define a sample implies the choice of an underlying assumption about the distribution of the population. The solution, then, is to obtain information about the underlying distribution of dates. This would require significantly more single-grain analyses than traditionally obtained.

5.3. Observed skew of date distribution

To examine the nature of single-grain date dispersion in more detail, we analyzed 25 grains for one sample in each transect (BAR-

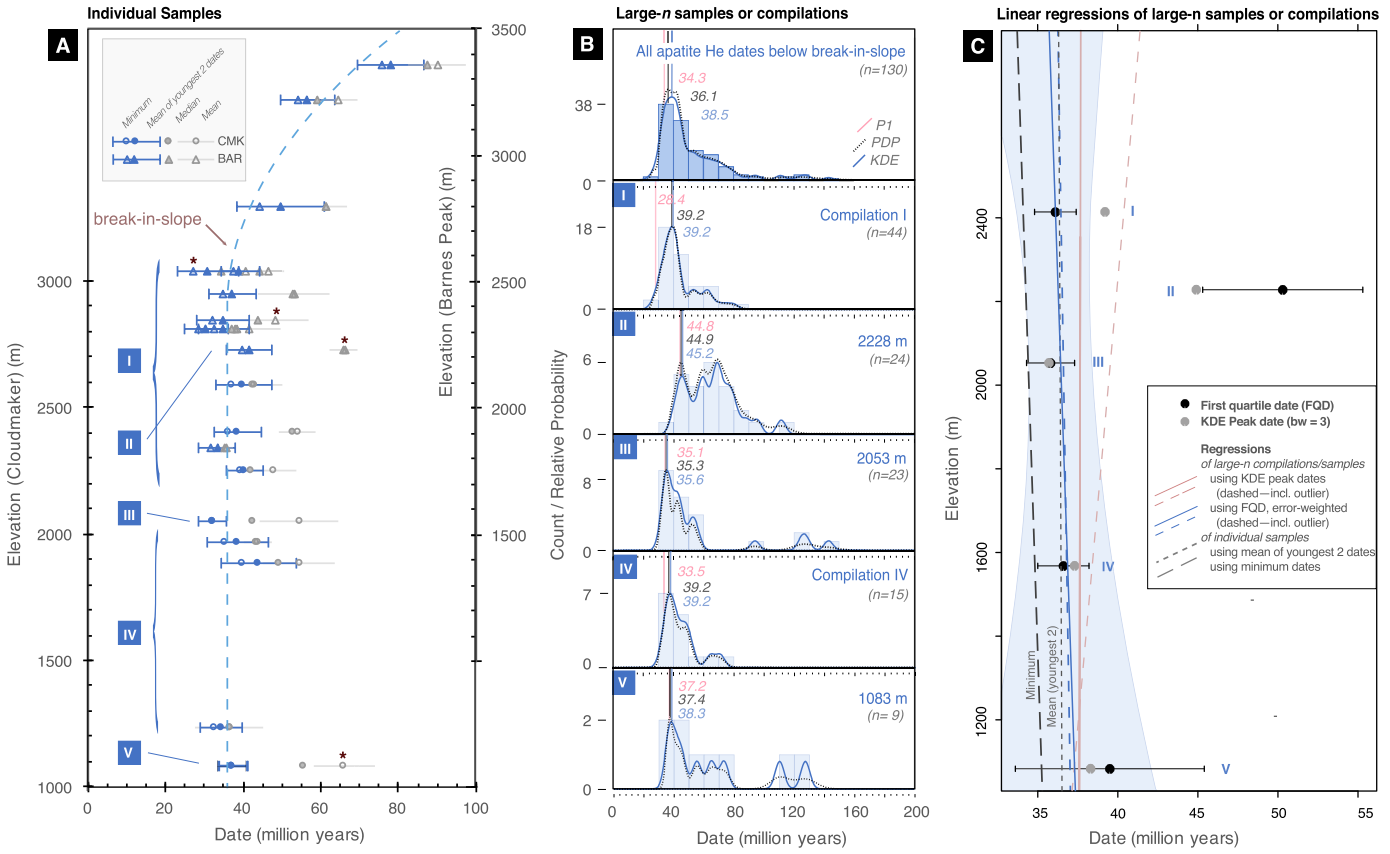

Fig. 3. Date-elevation transects of the Cloudmaker and Barnes Peak vertical transects and probability density distributions of individual and compiled samples. **(a)** Date-elevation relationship of individual samples, showing mean, median, mean of youngest two dates, and the minimum date of each sample; dashed line below break-in-slope indicates interpretation of the date-elevation trend, based on least square linear regressions in Fig. 3c. Note that data from the two vertical transects are shown on offset y-axes, indicating potential effect of tilting. Asterisks (*) indicate samples for which we noted potential impact of heterogeneous parent nuclide distribution or anomalies (see Supp. Fig. 1). Roman numerals correspond to labels in both panels (b) and (c). Sample CMK-2053 ("III"), the approximate midpoint between the lowermost sample ("V") and the break-in-slope, was used to divide the samples into adjacent-elevation groupings ("I"; "IV"). **(b)** Histograms, kernel density estimates (KDE; bandwidth = 3), and probability density distributions (PDP) for individual or combined samples; groupings as indicated by roman numerals in panel a. The distributions show that despite large date dispersion, late Eocene peak dates are consistent in samples below the break-in-slope for both the Barnes Peak and Cloudmaker transects, regardless of how samples are grouped. Peak dates are shown for the PDP, KDE, and youngest component fit (P1) assuming a 5-component mixture; see supplement for detail. **(c)** Peak dates and first quartile dates (with bootstrapped uncertainty, 1-σ) of distributions "I" through "V", plotted against elevation. For sample compilations, the midpoint of the elevation range is plotted on the y-axis. Linear regressions are based on either individual samples (black dashed—minimum dates; black dotted—mean of youngest two), or on large-n compilations (blue—first quartile date; red—KDE peak date). Blue uncertainty envelope corresponds to the solid blue line. See supplement for more detailed discussion of the bootstrap uncertainty estimates and linear regressions.

2228; CMK-2053), and 10 grains in one other sample (CMK-1083). We also composited data from smaller-n samples ($n \approx 5$) that are adjacent to each other in elevation (Fig. 3b). Because these individual samples have too few analyses to determine a reliable peak date, we used the large-n distributions to guide our interpretation of the small-n samples. The observed distributions confirm our expectations that dates are old-skewed with young peaks. The one exception is sample BAR-2228, which contained many grains with low-eU rims and exhibited a possible date-eU trend (Supp. Fig. 1, 5a). In general, the youngest kernel density estimate (KDE) peaks of these large-n distributions are ~37 Ma, while finite mixture modeling suggest slightly younger component dates of ~34 Ma (Fig. 3b). Given that the peak date of these distributions represents the most likely time of cooling through the apatite He closure temperature (for fast-cooled samples that are least affected by date variation due to eU and grain size), statistics that best estimate this peak such as the minimum or the first quartile date (FQD) represent the most geologically meaningful information for small-n samples. Because the FQD for the date distributions (except BAR-2228) are only 3-8% greater than the KDE peak (Fig. 3c), they provide a useful maximum age constraint (for a sample of five grains, the median-exclusive FQD is the mean of the youngest two grains).

A key benefit to larger-n analyses is that we can use the distributions to evaluate the behavior of summary statistics for varying sample sizes by bootstrapping and random subsampling (see Supplementary Material). By repeatedly drawing random subsets of n dates from the sample distribution (assuming it to be representative of the parent date distribution), we can consider how statistics like the mean, minimum, or FQD would vary every time we analyze different aliquots of n grains. As expected for old-skewed distributions with young peaks, estimates of FQD are more precise and accurate than estimates of the mean or median for any given sample size. For small sample sizes (n=5), the minimum date best estimates the young peak (Supp. Fig. 8), whereas for larger samples (n=25), the FQD becomes a better choice and the minimum can substantially underestimate the peak date. Because the minimum tends to decrease as n increases, one must be careful in its use when comparing samples of varying sizes.

The bootstrapped distributions further allow us to compute uncertainty estimates without additional assumptions about the underlying distribution (e.g. normality). In general, for any samples that have skewed population distributions similar to that observed here (e.g. CMK-2053, Fig. 3b), the 1σ-uncertainty in estimates of FQD from analyzing would be ~10-14% for n=5, and ~4-6% for n=25, whereas the uncertainties for the mean or median are 2-

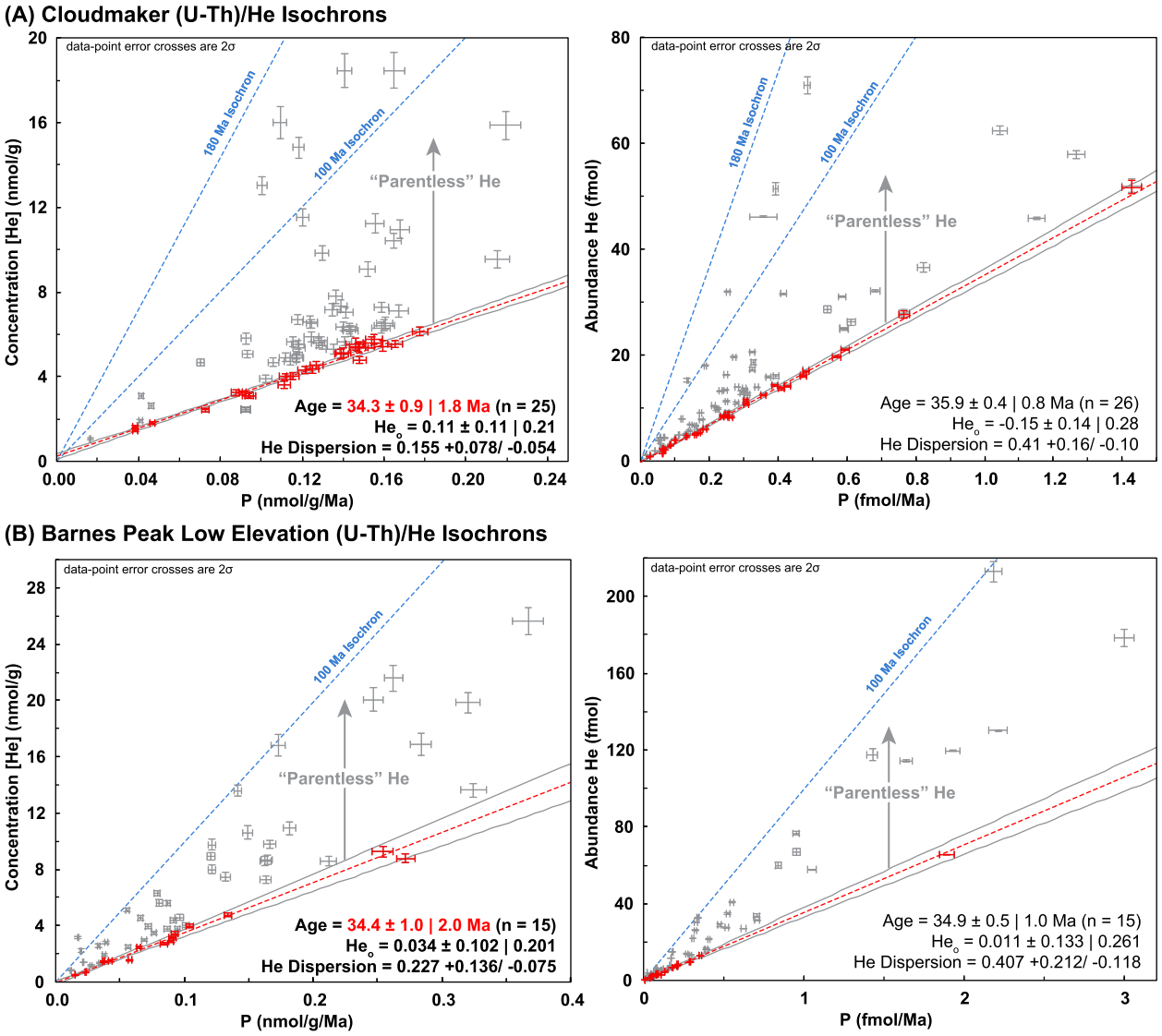

Fig. 4. Abundance-production and concentration-production plots of data from the Cloudmaker transect (a) and lower-elevation Barnes Peak samples below the break-in-slope (b). Isochrons are defined by the linear function t=[He]/P, where [He] is the abundance (fmol) or concentration (nmol/g) of helium, and P is the present day production rate of helium, a function of [U], [Th], and [Sm] (after Vermeesch, 2008). Isochron fits are from IsoplotR Model 3 Fit (including overdispersion), using the selected data points indicated in red. Notice that the youngest dates are distributed across a wide range of eU, and that older dates are not restricted to certain production ranges (i.e. eU ranges), suggesting that the cause of date anomalies is not correlated with eU (e.g. low eU grains gaining uranium, or high eU grains losing helium). The maximum dates define older isochrons (c. 180 Ma) that may be geologically meaningful. In this case, "parentless" He may actually represent radiogenic He trapped in inclusions or microvoids (Zeitler et al., 2017) and thus not be susceptible to diffusion until temperatures much higher than typical closure temperatures. The older isochron could thus represent a higher temperature thermal or cooling event, such as extensive Ferrar basalt intrusions at 180 Ma.

3 times higher. Thus, skewed distributions will frequently appear to be "overdispersed" when few grains are analyzed, with sample means reporting within 10% of the peak date in fewer than 20% of cases. This explains the apparent inconsistency in data when measures of central tendency are used to represent samples with skewed distributions (gray data points, Fig. 3a). At the same time, even with just five grains, the FQD and minimum date reliably estimate the KDE date peak by $<10\%$ in $>75\%$ of cases (on average, by $+3\%$ and -2%, respectively).

While we can use the distribution of individual large-n samples or compilations to inform analyses of smaller-n samples, a caveat is that not all samples in a vertical transect necessarily have the same-shaped date distribution. If all samples share a similar primary lithology, then such an assumption would be more appropriate, because they likely share a common set of characteristics that similarly affect apatite He date dispersion. If there are indications that certain sources of date discrepancy are dominant (e.g. large number of accessary minerals or grain boundary phases or coatings, systematic pattern of zonation, date-eU variation), as is the case in this study for sample BAR-2228, then they would exhibit different distributions. For this reason, identifying peak dates in large-n analyses ($n \approx 25$) for select samples located throughout a transect (e.g. top, middle, bottom) provides a way to corroborate age interpretation of smaller-n samples between these key samples, thus avoiding the time and expense of doing large-n analyses on all samples.

6. Discussion

6.1. Rapid exhumation across the Eocene-Oligocene transition

The probability distributions of dates below the break-in-slope of the date-elevation transect (Fig. 3b) demonstrate that there is more clarity in the data than would appear if we simply consider

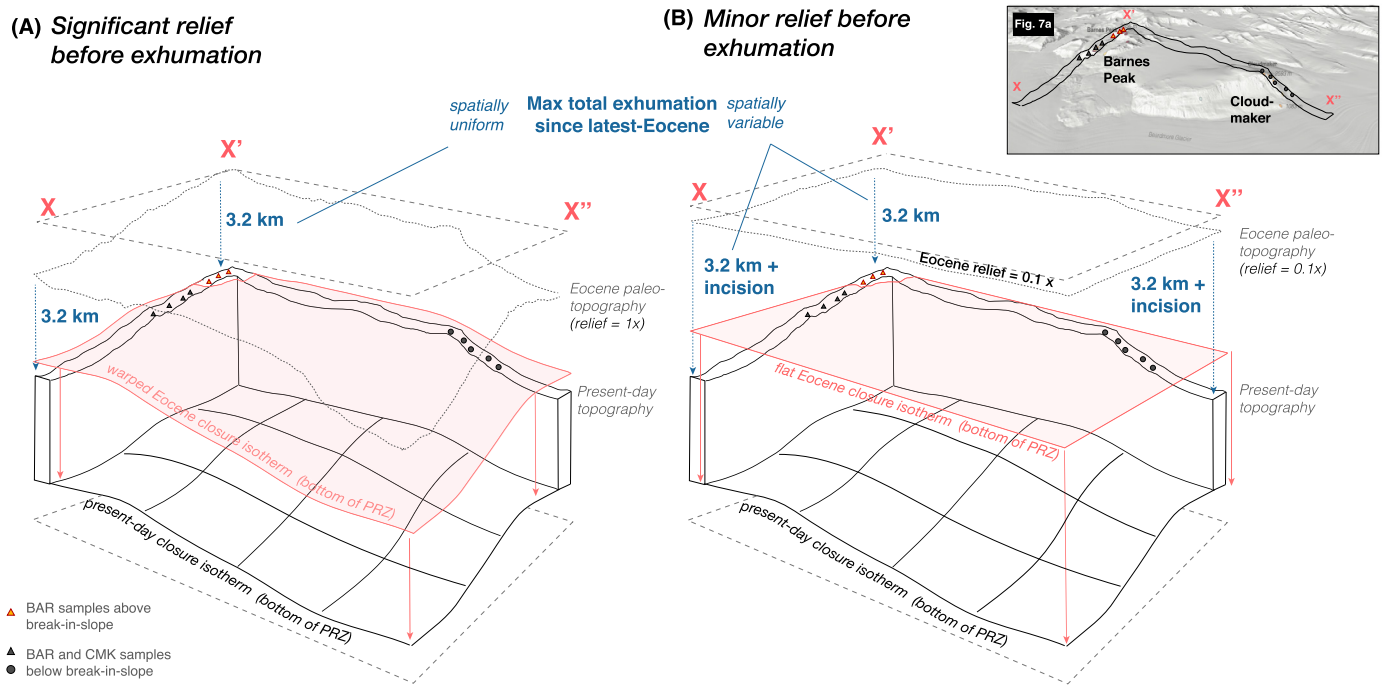

Fig. 5. Schematic block diagrams showing maximum total exhumation from the latest Eocene to now. The two end-member diagrams each shows modern topography (with the corners corresponding to X, X' and X" in the inset figure), the locations of Barnes Peak and Cloudmaker samples (samples above the break-in-slope are colored orange), and the present-day closure isotherm (gridded surface). The paleo-closure-isotherm (transparent red surface) is warped by the paleo-topography (dotted surface), which has either present-day relief (A) or 0.1 x present-day relief (B) just before exhumation. At any given point, the total exhumation since the latest Eocene is the difference between paleo- and current topography (blue arrow) or, equivalently, the difference between paleo- and current closure isotherms (red arrow). In either case, the preservation of the partial retention zone at Barnes Peak allows no more than 3.2 km of erosion (assuming geotherm of 25 C/km or greater) at that location. If modern-day topographic relief was reached prior to exhumation, this implies that a maximum of 3.2 km of erosion has occurred everywhere (A). If topographic relief has increased significantly during or after exhumation (B), then that maximum amount would be spatially variable (e.g. a glacial trough that is z km below the preserved-PRZ at Barnes Peak would have been exhumed at most 3.2+z km since the latest Eocene.

a small number of single-grain dates. Linear regression of the mean of the youngest two grains for individual samples closely match regressions of the FQD of large-n distributions (error weighted), and of peak dates (Fig. 3c), suggesting very rapid exhumation beginning no earlier than 37±2 Ma. Regression of the minimum dates in each sample constrains the onset of exhumation be no later than 34±3 Ma (Supp.). This is supported by the similar 34±2 Ma minimum isochron fits obtained from the concentration-production relationships (Fig. 4). The slope of the date-elevation relationship (DER) reflects an apparent exhumation rate of no less than 0.4 mm/a (95% CI) (Fig. 3c), though the upper bound is unconstrained because of the near-vertical slope of the DER.

The presence of a break-in-slope of the DER (Fig. 3a) near the top of the Barnes Peak transect provides a critical constraint, recording the preserved ~80 °C base of the former apatite He PRZ before the onset of rapid exhumation (Fig. 3a). This signifies 3.2-2.3 km of total exhumation since the latest Eocene from above ~2600 m at Barnes Peak (Fig. 5a), assuming a geothermal gradient of 25-35 °C/km. If most of the relief was created after late Eocene, the estimate of total exhumation elsewhere will be greater at sites that have been eroded more, relative to the preserved break-in-slope at Barnes Peak (Fig. 5b). Thus, this amount is consistent with exhumation estimates of ~4.2 km at the peak of the Cloudmaker, approximated from the thickness of eroded sedimentary units, sills, and basalt flows still present elsewhere (Fitzgerald, 1994). Similarly, this amount implies 7.8-6.9 km of incision since the latest Eocene at the Beardmore trough, and up to 8.8 km near the Cloudmaker where the trough has been overdeepened to ~2 km below sea level (Supp. Material). Finally, we note that it is extremely unlikely (<1%, assuming a probability distribution of dates as discussed above) that this break-in-slope reflects sparse sampling that simply missed younger apatite grains, given that no samples above it yielded any single-grain dates <40 Ma.

The date-elevation transect further constrains the magnitude of rapid exhumation that started at c. 37-34 Ma. This is represented by the near-vertical portion of the DER below the break-in-slope, which has an absolute elevation difference of 1.5 km (from the lowermost Cloudmaker sample to the base of the Barnes Peak PRZ), or 2.6 km when restoring for syn- and post-exhumational flexural isostatic tilting relative to the tilted Kukri Peneplain (Supp. Tables). If topographic relief during the latest Eocene were minor, and isotherms were essentially flat, then this would require at least 1.5-2.6 km of rapid exhumation. However, because deeply-incised topography warps lower-temperature isotherms, any pre-existing topography before exhumation or any increase of relief during exhumation must be accounted for when calculating exhumation rate or magnitude (Mancktelow and Grasemann, 1997). Different assumptions about the temporal and spatial variability of exhumation would thus lead to slightly different estimates. Fig. 6 illustrates the various endmember scenarios for these calculations. At minimum, even if we assume that full modern-day topographic relief was already achieved by the latest Eocene, the near-vertical DER of the Cloudmaker transect alone still constrains exhumation to be >1.4 km during latest Eocene (Fig. 6A-1). If we further assume that regional tilting occurred after exhumation (for example, due to isostatic rebound associated with glacial incision; Stern, 2005), then the data require >1.6 km of exhumation (Fig. 6A-2). Though fluvial valleys likely preceded glaciation, significant over-deepening of the Beardmore trough was almost certainly accomplished by glacial erosion. Thus, the most reasonable estimate would be >2.6 km (Fig. 6B-4). Note that these are minimum estimates because the lower limit of the DER is unconstrained, as the bedrock below the lowest-sampled outcrop is ice-covered.

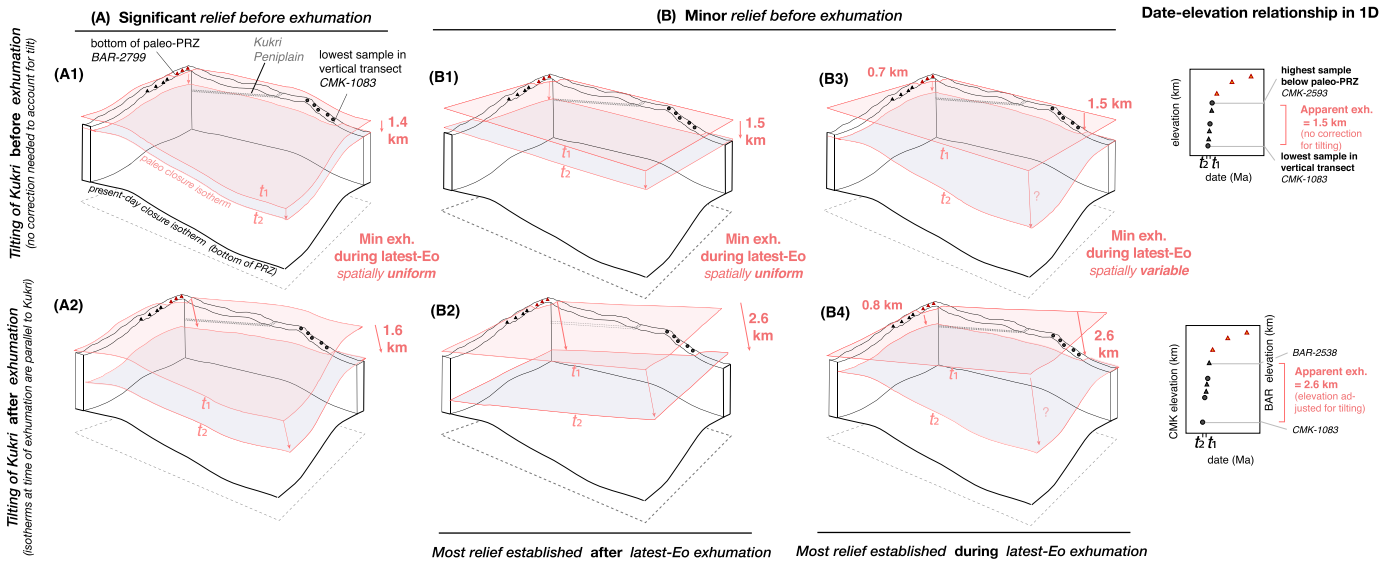

Fig. 6. End-member scenarios showing how different assumptions of temporally and spatially variable exhumation affects the interpretation of apatite helium dates in three dimensions. From a fixed reference frame, the effect of erosional exhumation can be visualized as the passage of the closure isotherm surface through a stationary crustal block. Depending on the initial shape and tilt of the surface, and how that changes during exhumation, the same data (projected in one-dimension as a date-elevation transect) give varying constraints on the magnitude of exhumation. Note that scenarios (A1-2) and (B1-4) correspond to diagrams (A) and (B) in Fig. 5, respectively. The red and blue transparent surfaces represent the positions of the paleo-closure-isotherm at times t_1 and t_2, which correspond to the top and bottom of the near-vertical portion of the date-elevation relationship. See supplementary material for details of minimum constraint calculation for each endmember scenario, and additional confirmation of the effect of incision on the spatial pattern of apatite helium data using 3D thermo-kinematic modeling.

We conclude that the date-elevation transects provide direct evidence of >2.6 km of incision near the Cloudmaker, occurring within 3-6 million years during the latest Eocene to earliest Oligocene. Although the exact timing has some uncertainty, onset of enhanced erosion was clearly coeval with either the growth of the Antarctic ice-sheet at the Eocene-Oligocene transition or the development of regional glaciation just before the transition. This is significantly younger than previous estimates for the onset of erosion in the central TAM (Fitzgerald et al., 2006; Miller et al., 2010), and implies that glacial incision may have been a primary driver of uplift and exhumation of the TAM.

6.2. Post-Eocene extension and flexural uplift of the TAM rift flank

In addition to cooling associated with exhumation by glacial erosion, our new apatite He data also record enhanced footwall exhumation related to rifting at the TAM front. Normal faulting can cause cooling either directly through tectonic unroofing of the hanging wall, and/or by focused erosion of topography created by footwall flexural isostatic uplift of the TAM rift flank (Ehlers, 2005). The lack of any significant vertical offset of the Kukri Peneplain along or across the Beardmore Glacier trough implies inland exhumation was not directly associated with any adjacent faults. Instead, this exhumation likely reflects erosion in response to flexural isostatic uplift. A previous AFT study within 30 km of the Shackleton Glacier mouth inferred that accelerated exhumation of 4.9-6.0 km since c. 45 Ma was the direct erosional response to rift-related footwall uplift (Miller et al., 2010). Our new apatite He dataset shows that significant exhumation actually extends at least 100 km inboard from the TAM front along the Beardmore Glacier (Fig. 6b), with the onset of rapid exhumation starting later at around the Eocene-Oligocene transition. Such exhumation so far inland is significant, because the distance over which flexural isostatic uplift and associated exhumation decays over long distances, with the greatest uplift and exhumation concentrated at the TAM front (Stern et al., 2005). Furthermore, rift-related uplift alone cannot explain the higher amounts of total exhumation further inland compared to the Shackleton Glacier. Instead, models show that the higher uplift and exhumation along the Beardmore trough must reflect additional flexural isostatic rebound in response to deeper localized glacial incision by the Beardmore Glacier relative to the Shackleton Glacier (Stern et al., 2005) since the latest Eocene.

6.3. Additional exhumation in the Oligocene

Samples from the U.S. Polar Rock Repository allowed deeper and wider sampling to extend our record beyond the elevation transects (Figs. 2; 7). These data show similar date dispersion, but unlike the dataset from the densely sampled transects, they do not provide enough spatial resolution for a similarly detailed analysis. One broad observation is that the majority of samples from 0 to 900 m yielded late Oligocene to early Miocene minimum dates or FQD (Supp. Fig. 11). To assess the significance of these younger ages despite the paucity of analyses, we compiled single-grain He data from all samples from the central TAM and examined the probability distribution of the entire dataset. If a simplistic crustal block with minor topography is evenly sampled in three dimensions such that all elevations are equally represented, then intervals of rapid exhumation will appear as prominent peaks in the compiled dataset because a greater volume of crust will have passed through the closure isotherm during a time interval of rapid exhumation than at an equivalent interval of slow exhumation. Similarly, if the compiled dataset of all samples in the study area is weighted such that all elevations are equally represented, we can then evaluate the relative frequency of cooling dates in the entire study area (Fig. 8a). We emphasize that this approach discounts important factors such as relief and differential uplift/tilting that are necessary for detailed analysis of closely spaced samples, and provides only a regional, first-order overview of cooling dates.

The resulting elevation-weighted date distribution reveals two peaks in the late Eocene and in the late Oligocene (Fig. 8). While other older, pre-Eocene peaks may be artifacts of the combined effects of poor sampling resolution at higher elevations and of old-skewed dates from younger samples, these two peaks are clear evidence that certain cooling dates are over-represented in the bedrock record. The late Eocene peak is expected, based on the results from the elevation transects (Section 6.1). The late Oligocene peak is not immediately apparent in the unweighted compilation,

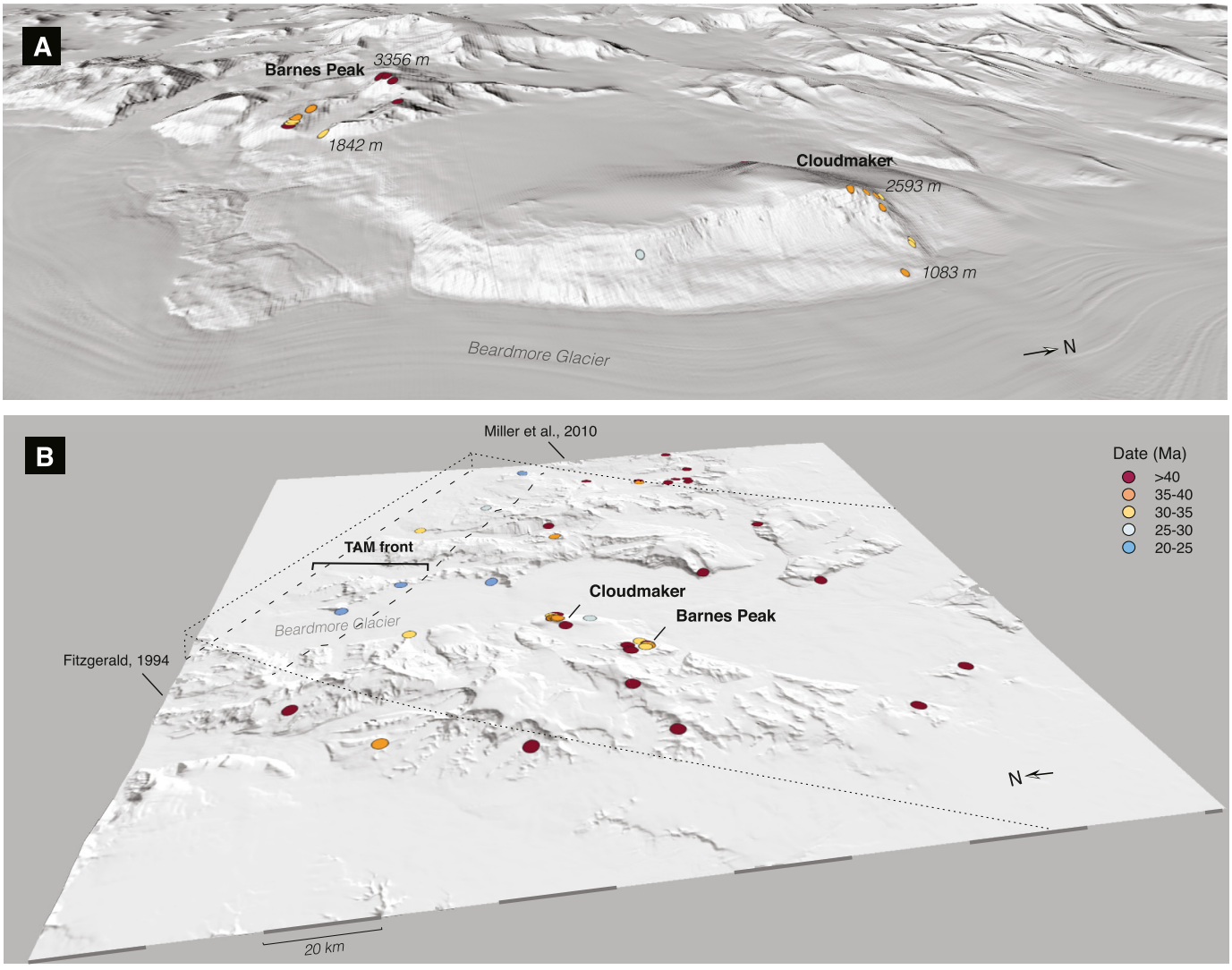

Fig. 7. Spatial distribution of apatite He cooling dates. **(a)** View of Barnes Peak and Cloudmaker transects (elevation of top and bottom of each transect indicated for scale); **(b)** View of study area (no vertical exaggeration), showing the approximate location of previous apatite fission track studies along the Transantarctic Mountain (TAM) front (Fitzgerald, 1994; Miller et al., 2010) relative to the Cloudmaker and Barnes Peak transects. The color scale for cooling dates are the same for both panels, and indicate the mean of the youngest two grains. Flexural-isostatic uplift along the TAM rift flank is shown schematically (cf. Stern 2005). Each edge of the domain is 205 km.

but appears prominently in the elevation-weighted compilations (Fig. 8a). The prevalence of ~25-20 Ma cooling dates could reflect a significant pulse of exhumation during the late Oligocene, or alternatively, steady erosion throughout the Oligocene until mid-Miocene, if topographic relief has not changed significantly since that time. More analyses and denser sampling to fully evaluate the effect of paleo-topography would be key to distinguishing between these scenarios.

6.4. Does enhanced erosion correlate with periods of higher temperature?

The onset of rapid exhumation around the Eocene-Oligocene transition raises the question of whether enhanced exhumation is generally coupled with changes in cryosphere conditions during key climatic transitions. Also notable is the prevalence of late Oligocene cooling dates in the elevation-weighted compilation, which coincide with the longest interval of warming and minimum ice volume during Oligocene, from 24.2 to 23.7 Ma, whereas there are fewer cooling dates during the relatively colder Mid-Oligocene Glacial Interval, even though this period is also associated with significant, cyclic ice-volume fluctuations (Fig. 8) (Liebrand et al., 2017). Furthermore, both the late Eocene and late Oligocene cooling date peaks coincide with times when benthic foraminiferal $\delta^{18}O$ values crossed ~1.4-1.6‰, the bounding limit dividing a potentially ice-free world and one with permanent ice-sheets (Fig. 8). One reasonable hypothesis is that glacial erosion rates were not uniformly high from 34-14 Ma, but were rather enhanced when temperature was elevated above a certain threshold.

An important point is that enhanced erosion during these times would not require widespread glacial erosion. Indeed, studies elsewhere in East Antarctica have documented little exhumation since the Paleozoic (Cox et al., 2010; Rolland et al., 2019). Instead, enhanced erosion could be attributed to localized, highly-erosive glaciers with temperate thermal regimes cutting across pre-existing topography of the TAM. In fact, the most erosive glaciers today, such as those in Southeast Alaska and Patagonia that exhibit erosion rates on the order of $10^0 \sim 10^1$ mm/a (km/Ma), are found in areas with warmer temperatures (mean annual temperature of 5-9 °C) and high precipitation compared to less erosive glaciers with polar or subpolar thermal regimes (Cowan et al., 2010; Boldt et al., 2013; Koppes et al., 2015). Warm conditions allow abundant surface meltwater to create conduits that supply subglacial streams, facilitating sediment evacuation

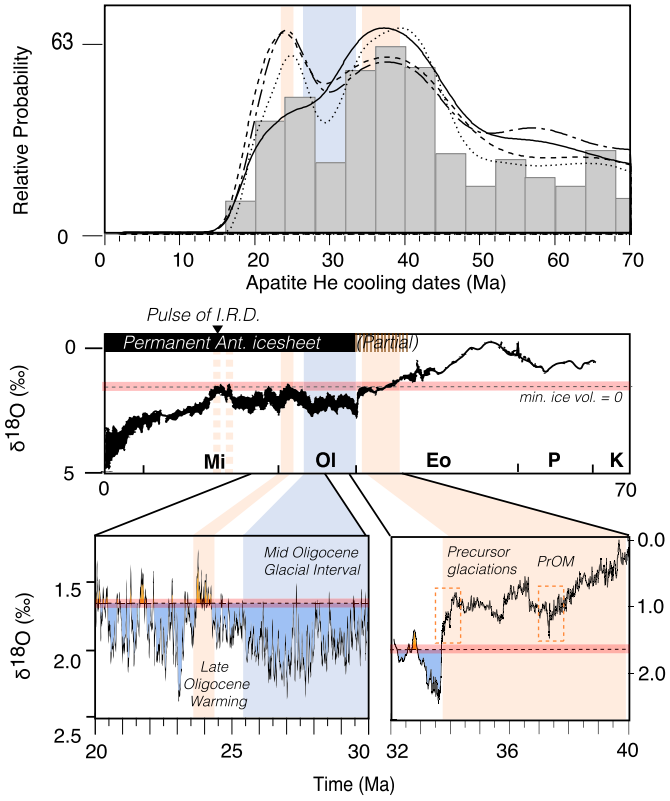

Fig. 8. Correlation between Cenozoic cooling dates and oxygen isotopic data. **(a)** histogram and probability density plots of elevation-weighted dataset of compiled apatite helium data from this study (dotted line — 500-m binned resampling; dashed — 250-m binned resampling; dash-dotted—running resampling; solid— unweighted; see supplement for detail). Additional large-n analyses (beyond the first 5 grains in each sample) are excluded so no single sample is overrepresented, though similar results are obtained if they are included. **(b)** simplified oxygen isotope stack from Zachos et al. (2008); vertical orange bars indicate times when oxygen isotope value approached a threshold of ~1.4-1.6‰, indicated by horizontal line. Timing of Miocene pulse of ice-rafted debris (IRD) from Pierce et al., 2017. **(c)** High resolution oxygen isotopic record from benthic foraminifera from Liebrand et al. (2017) and Scher et al. (2014); red line indicates approximate limit of potentially ice-free conditions (minimum ice volume contribution = 0) assuming minimum bottom water temperature of 2.5 °C and $\delta^{18}O_{ice}$ value of −42‰ VSMOW (Liebrand et al., 2017). (PrOM — Priabonian Oxygen Isotope Maximum).

and increasing erosive power (Koppes et al., 2015; Alley et al., 2019). Similarly temperate conditions likely prevailed in the TAM during late Eocene and late Oligocene, when $\delta^{18}O$ values of ~1.4-1.6‰ approximately correspond to mean temperatures of 5-6 °C in an ice-free ocean (Zachos et al., 2008). Further investigation of this hypothesis requires additional data from more detailed vertical transects and lower-temperature thermochronometers. If it is valid, other times of elevated temperature since the inception of the EAIS, e.g. the Mid-Miocene Climatic Optimum, should also be associated with enhanced exhumation.

7. Conclusions

- Large intrasample dispersion of bedrock-derived apatite He dates often cannot be explained by known sources of date variation or analytical error. In such cases, using measures of central tendency can lead to the appearance of uninterpretable data. However, we show that the youngest peaks of dispersed, skewed date probability density distributions correspond to the time of cooling in fast-cooled samples, and such peaks can be estimated using the minimum or first quartile date.
- For similarly dispersed datasets that do not exhibit date-eU or date-size correlations indicative of slow cooling, robust age interpretation requires sufficient data (n ≈ 25) to characterize the probability distribution of dates for at least two or three samples (e.g. top, middle, bottom of a transect). Instead of basing interpretation on the assumption that single-grain dates in a sample would be normally distributed, this allows selection of the most appropriate summary statistics and calculation of their uncertainty based on empirical distributions. These distributions can thus be used to inform interpretation of more closely spaced, smaller-*n* samples in between the larger-*n* samples.
- Using this workflow, we show that date-elevation transects on the west side of the Beardmore Glacier in the TAM yield direct evidence of at least 2.6 km of rapid exhumation around the Eocene-Oligocene transition, at a rate of no less than 0.4 mm/a. This is significantly younger than previous estimates of early Eocene exhumation in this area.
- The preservation of a paleo-partial retention zone limits total exhumation since ~37-34 Ma to be 3.2 km at the top of Barnes Peak and up to 8.8 km at the deepest part of the Beardmore trough.
- 20-25 Ma cooling dates are prevalent at lower elevations closer to the TAM front, which could be explained by enhanced late Oligocene exhumation, or steady exhumation over a longer period of time.
- We note potential correlations between the timing of rapid exhumation and key climatic transitions, especially the onset of Antarctic glaciation at the Eocene-Oligocene Transition. During late Oligocene, relatively warmer temperatures above threshold conditions may have maximized erosion by increasing subglacial meltwater.

CRediT authorship contribution statement

John He: Conceptualization, Data curation, Formal analysis, Investigation, Visualization, Writing – original draft. **Stuart N. Thomson:** Conceptualization, Formal analysis, Funding acquisition, Investigation, Writing – review & editing. **Peter W. Reiners:** Conceptualization, Formal analysis, Funding acquisition, Investigation, Methodology, Writing – review & editing. **Sidney R. Hemming:** Conceptualization, Funding acquisition, Investigation, Writing – review & editing. **Kathy J. Licht:** Conceptualization, Funding acquisition, Investigation, Writing – review & editing.

Declaration of competing interest

The authors declare that they have no known competing financial interests or personal relationships that could have appeared to influence the work reported in this paper.

Acknowledgements

We thank Christine Kassab for the contribution of additional data (samples PRR-26003, 5862, 29990, 6120, 34583), and Uttam Chowdhury and Alex Pritika for assistance with apatite He analyses. We are grateful to the U.S. Antarctic Program staff, mountaineer Dennis Haskell, pilots from PHI, and the Shackleton Deep Field Camp staff for field assistance. This work was supported by NSF Office of Polar Program (OPP) award 1443556 (Thomson and Reiners), 1043572 (Licht), 1443565 (Hemming), and the John Mason Clarke 1877 fellowship (He). Aerial photograph and DEM were made available by the Polar Geospatial Center, supported by NSF-OPP awards 1543501, 1810976, 1542736, 1559691, 1043681, 1541332, 0753663, 1548562, 1238993, NASA award NNX10AN61G, the Blue Waters Innovation Initiative, and data from DigitalGlobe, Inc. Polar Rock Repository samples were provided by the Byrd Polar and Climate Research Center with support from the National Science Foundation, under Cooperative Agreement OPP-1643713.

Appendix A. Supplementary material

Supplementary material related to this article can be found online at https://doi.org/10.1016/j.epsl.2021.117009.

References

Alley, R.B., Cuffey, K.M., Zoet, L.K., 2019. Glacial erosion: status and outlook. Ann. Glaciol. 60, 1–13. https://doi.org/10.1017/aog.2019.38.

Ault, A.K., Flowers, R.M., 2012. Is apatite U–Th zonation information necessary for accurate interpretation of apatite (U–Th)/He thermochronometry data? Geochim. Cosmochim. Acta 79, 60–78. https://doi.org/10.1016/j.gca.2011.11.037.

Boldt, K.V., Nittrouer, C.A., Hallet, B., Koppes, M.N., Forrest, B.K., Wellner, J.S., Anderson, J.B., 2013. Modern rates of glacial sediment accumulation along a 15° S-N transect in fjords from the Antarctic peninsula to southern Chile. J. Geophys. Res., Earth Surf. 118, 2072–2088. https://doi.org/10.1002/jgrf.20145.

Brown, R.W., Beucher, R., Roper, S., Persano, C., Stuart, F., Fitzgerald, P., 2013. Natural age dispersion arising from the analysis of broken crystals. Part I: Theoretical basis and implications for the apatite (U-Th)/He thermochronometer. Geochim. Cosmochim. Acta 122, 478–497. https://doi.org/10.1016/j.gca.2013.05.041.

Cooperdock, E.H.G., Ketcham, R.A., Stockli, D.F., 2019. Resolving the effects of 2D versus 3D grain measurements on (U-Th)/He age data and reproducibility. Geochronol. Discuss. 1 (32). https://doi.org/10.5194/gchron-2019-3.

Cowan, E., Seramur, K., Powell, R., Willems, B., Gulick, S., Jaeger, J., 2010. Fjords as temporary sediment traps: history of glacial erosion and deposition inMuir Inlet, Glacier Bay National Park, southeastern Alaska. Geol. Soc. Am. Bull. 122, 1067–1080.

Cox, S.E., Thomson, S.N., Reiners, P.W., Hemming, S.R., Van de Flierdt, T., 2010. Extremely low long - term erosion rates around the Gamburtsev Mountains in interior East Antarctica. Geophys. Res. Lett. 37, 3–7. https://doi.org/10.1029/2010GL045106.

Ehlers, T.A., 2005. Crustal thermal processes and the interpretation of thermochronometer data. Rev. Mineral. Geochem. 58, 315–350. https://doi.org/10.2138/rmg.2005.58.12.

Farley, K.A., 2000. Helium diffusion from apatite: general behavior as illustrated by Durango fluorapatite. J. Geophys. Res., Solid Earth 105 (B2), 2903–2914.

Farley, K.A., 2002. (U-Th)/He dating: techniques, calibrations, and applications. Rev. Mineral. Geochem. 47, 819–844. https://doi.org/10.2138/rmg.2002.47.18.

Farley, K.A., Shuster, D.L., Ketcham, R.A., 2011. U and Th zonation in apatite observed by laser ablation ICPMS, and implications for the (U-Th)/He system. Geochim. Cosmochim. Acta 75, 4515–4530. https://doi.org/10.1016/j.gca.2011.05.020.

Farley, K.A., Stockli, D.F., 2002. (U-Th)/ He dating of phosphates. Rev. Mineral. Geochem. 15, 559–577. https://doi.org/10.2138/rmg.2002.48.15.

Fitzgerald, P.G., 1994. Thermochronologic constraints on post-Paleozoic tectonic evolution of the central Transantarctic Mountains, Antarctica. Tectonics 13, 818–836. https://doi.org/10.1029/94TC00595.

Fitzgerald, P.G., 1992. The transantarctic mountains of southern Victoria land: the application of apatite fission track analysis to a rift shoulder uplift. Tectonics 11, 634–662.

Fitzgerald, P.G., Baldwin, S.L., Webb, L.E., O'Sullivan, P.B., 2006. Interpretation of (U-Th)/He single grain ages from slowly cooled crustal terranes: a case study from the Transantarctic Mountains of southern Victoria Land. Chem. Geol. 225, 91–120. https://doi.org/10.1016/j.chemgeo.2005.09.001.

Fitzgerald, P.G., Stump, E., 1997. Cretaceous and Cenozoic episodic denudation of the Transantarctic Mountains, Antarctica: New constraints from apatite fission track thermochronology in the Scott Glacier region. J. Geophys. Res. 102, 7747–7765.

Flowers, R.M., Kelley, S.A., 2011. Interpreting data dispersion and "inverted" dates in apatite (U-Th)/He and fission-track datasets: An example from the US midcontinent. Geochim. Cosmochim. Acta 75, 5169–5186. https://doi.org/10.1016/j.gca.2011.06.016.

Flowers, R.M., Farley, K.A., Ketcham, R.A., 2015. A reporting protocol for thermochronologic modeling illustrated with data from the Grand Canyon. Earth Planet. Sci. Lett. 432, 425–435. https://doi.org/10.1016/j.epsl.2015.09.053.

Flowers, R.M., Ketcham, R.A., Shuster, D.L., Farley, K.A., 2009. Apatite (U-Th)/He thermochronometry using a radiation damage accumulation and annealing model. Geochim. Cosmochim. Acta 73, 2347–2365. https://doi.org/10.1016/j.gca.2009.01.015.

Francis, J.E., Marenssi, S., Levy, R., Hambrey, M., Thorn, V.C., Mohr, B., Brinkhuis, H., Warnaar, J., Zachos, J., Bohaty, S., DeConto, R., 2008. Chapter 8 From Greenhouse to Icehouse - The Eocene/Oligocene in Antarctica. Dev. Earth Environ. Sci. 8, 309–368. https://doi.org/10.1016/S1571-9197(08)00008-6.

Galeotti, S., DeConto, R., Naish, T., Stocchi, P., Florindo, F., Pagani, M., Barrett, P., Bohaty, S.M., Lanci, L., Pollard, D., Sandroni, S., Talarico, F.M., Zachos, J.C., 2016. Antarctic Ice Sheet variability across the Eocene-Oligocene boundary climate transition. Science 80 (352), 76–80. https://doi.org/10.1126/science.aab0669.

Gasson, E., DeConto, R., Pollard, D., 2015. Antarctic bedrock topography uncertainty and ice sheet stability. Geophys. Res. Lett. 42, 5372–5377. https://doi.org/10.1002/2015GL064322.

Gautheron, C., Tassan-got, L., Barbarand, J., Pagel, M., 2009. Effect of alpha-damage annealing on apatite (U – Th)/ He thermochronology. Chem. Geol. 266, 157–170. https://doi.org/10.1016/j.chemgeo.2009.06.001.

Gautheron, C., Tassan-Got, L., Ketcham, R.A., Dobson, K.J., 2012. Accounting for long alpha-particle stopping distances in (U-Th-Sm)/He geochronology: 3D modeling of diffusion, zoning, implantation, and abrasion. Geochim. Cosmochim. Acta 96, 44–56. https://doi.org/10.1016/j.gca.2012.08.016.

Guenthner, W.R., Reiners, P.W., Chowdhury, U., 2016. Isotope dilution analysis of Ca and Zr in apatite and zircon (U-Th)/He chronometry. Geochem. Geophys. Geosyst. 17, 1623–1640. https://doi.org/10.1002/2016GC006311.

Gulick, S.P.S., Shevenell, A.E., Montelli, A., Fernandez, R., Smith, C., Warny, S., Bohaty, S.M., Sjunneskog, C., Leventer, A., Frederick, B., Blankenship, D.D., 2017. Initiation and long-term instability of the East Antarctic Ice Sheet. Nature 552, 225–229. https://doi.org/10.1038/nature25026.

Guo, H., Zeitler, P.K., Idleman, B., Fayon, A., 2019. Using continuous ramped heating to assess (u-th)/He age dispersion: a case study in transantarctic mountains. In: AGUFM. p. V11D–0122.

Harlov, D.E., 2015. Apatite: a fingerprint for metasomatic processes. Elements 11, 171–176. https://doi.org/10.2113/gselements.11.3.171.

Hochmuth, K., Gohl, K., Leitchenkov, G., Sauermilch, I., 2020. The evolving paleobathymetry of the circum - Antarctic Southern Ocean since 34 ma: a key to understanding past cryosphere - ocean developments geochemistry, geophysics, geosystems. Geochem. Geophys. Geosyst., 1–28. https://doi.org/10.1029/2020GC009122.

Idleman, B.D., Zeitler, P.K., McDannell, K.T., 2018. Characterization of helium release from apatite by continuous ramped heating. Chem. Geol. 476, 223–232. https://doi.org/10.1016/j.chemgeo.2017.11.019.

Jamieson, S.S.R., Sugden, D.E., Hulton, N.R.J., 2010. The evolution of the subglacial landscape of Antarctica. Earth Planet. Sci. Lett. 293, 1–27. https://doi.org/10.1016/j.epsl.2010.02.012.

Koppes, M., Hallet, B., Rignot, E., Mouginot, J., Wellner, J.S., Boldt, K., 2015. Observed latitudinal variations in erosion as a function of glacier dynamics. Nature 526, 100–103. https://doi.org/10.1038/nature15385.

Liebrand, D., de Bakker, A.T.M., Beddow, H.M., Wilson, P.A., Bohaty, S.M., Ruessink, G., Pälike, H., Batenburg, S.J., Hilgen, F.J., Hodell, D.A., Huck, C.E., Kroon, D., Raffi, I., Saes, M.J.M., van Dijk, A.E., Lourens, L.J., 2017. Evolution of the early Antarctic ice ages. Proc. Natl. Acad. Sci. 114, 3867–3872. https://doi.org/10.1073/pnas.1615440114.

Lindeque, A., Gohl, K., Wobbe, F., Uenzelmann-neben, G., 2016. Preglacial to glacial sediment thickness grids for the Southern Pacific Margin of West Antarctica. Geochem. Geophys. Geosyst. 17, 4276–4285. https://doi.org/10.1002/2016GC006401.Received.

Liu, Z., Pagani, M., Zinniker, D., DeConto, R., Huber, M., Brinkhuis, H., Shah, S.R., Leckie, R.M., Pearson, A., 2009. Global cooling during the Eocene-Oligocene climate transition. Science 80 (323), 1187–1190. https://doi.org/10.1126/science.1166368.

Mancktelow, N.S., Grasemann, B., 1997. Time-dependent effects of heat advection and topography on cooling histories during erosion. Tectonophysics 270, 167–195. https://doi.org/10.1016/S0040-1951(96)00279-X.

McDannell, K.T., Zeitler, P.K., Janes, D.G., Idleman, B.D., Fayon, A.K., 2018. Screening apatites for (U-Th)/He thermochronometry via continuous ramped heating: He age components and implications for age dispersion. Geochim. Cosmochim. Acta 223, 90–106. https://doi.org/10.1016/j.gca.2017.11.031.

Meesters, A.G.C.A., Dunai, T.J., 2002. Solving the production–diffusion equation for finite diffusion domains of various shapes: Part II. Application to cases with α-ejection and nonhomogeneous distribution of the source. Chem. Geol. 186, 57–73.

Miller, S.R., Fitzgerald, P.G., Baldwin, S.L., 2010. Cenozoic range-front faulting and development of the Transantarctic Mountains near Cape Surprise, Antarctica: thermochronologic and geomorphologic constraints. Tectonics 29, 1–21. https://doi.org/10.1029/2009TC002457.

Murray, K.E., Orme, D.A., Reiners, P.W., 2014. Effects of U-Th-rich grain boundary phases on apatite helium ages. Chem. Geol. 390, 135–151. https://doi.org/10.1016/j.chemgeo.2014.09.023.

Paxman, G.J.G., Jamieson, S.S.R., Hochmuth, K., Gohl, K., Bentley, M.J., Leitchenkov, G., Ferraccioli, F., 2019. Reconstructions of Antarctic topography since the Eocene – Oligocene boundary. Palaeogeogr. Palaeoclimatol. Palaeoecol. 535, 109346. https://doi.org/10.1016/j.palaeo.2019.109346.

Peyton, S.L., Reiners, P.W., Carrapa, B., Decelles, P.G., 2012. Low-temperature thermochronology of the northern Rocky Mountains, western U.S.A. Am. J. Sci. 312, 145–212. https://doi.org/10.2475/02.2012.04.

Pierce, E.L., van de Flierdt, T., Williams, T., Hemming, S.R., Cook, C.P., Passchier, S., 2017. Evidence for a dynamic East Antarctic ice sheet during the mid-Miocene climate transition. Earth Planet. Sci. Lett. 478, 1–13. https://doi.org/10.1016/j.epsl.2017.08.011.

Reiners, P.W., Farley, K.A., 2001. Influence of crystal size on apatite (U–Th)/He thermochronology: an example from the Bighorn Mountains, Wyoming. Earth Planet. Sci. Lett. 188, 413–420. https://doi.org/10.1016/S0012-821X(01)00341-7.

Roberts, A.P., Wilson, G.S., Harwood, D.M., Verosub, K.L., 2003. Glaciation across the Oligocene-Miocene boundary in southern McMurdo Sound, Antarctica:

new chronology from the CIROS-1 drill hole. Palaeogeogr. Palaeoclimatol. Palaeoecol. 198, 113–130. https://doi.org/10.1016/S0031-0182(03)00399-7.
Rolland, Y., Bernet, M., van der Beek, P., Gautheron, C., Duclaux, G., Bascou, J., Balvay, M., Héraudet, L., Sue, C., Ménot, R.P., 2019. Late Paleozoic Ice Age glaciers shaped East Antarctica landscape. Earth Planet. Sci. Lett. 506, 123–133. https://doi.org/10.1016/j.epsl.2018.10.044.
Scher, H.D., Bohaty, S.M., Smith, B.W., Munn, G.H., 2014. Isotopic interrogation of a suspected late Eocene glaciation. Paleoceanography 29, 628–644. https://doi.org/10.1002/2014PA002648.
Shuster, D.L., Flowers, R.M., Farley, K.A., 2006. The influence of natural radiation damage on helium diffusion kinetics in apatite. Earth Planet. Sci. Lett. 249, 148–161. https://doi.org/10.1016/j.epsl.2006.07.028.
Siegert, M.J., 2008. Antarctic subglacial topography and ice-sheet evolution. Earth Surf. Process. Landf. 33, 646–660. https://doi.org/10.1002/esp.1670.
Spiegel, C., Kohn, B., Belton, D., Berner, Z., Gleadow, A., 2009. Apatite (U-Th-Sm)/He thermochronology of rapidly cooled samples: the effect of He implantation. Earth Planet. Sci. Lett. 285, 105–114. https://doi.org/10.1016/j.epsl.2009.05.045.
Stern, T.A., Baxter, A.K., Barrett, P.J., 2005. Isostatic rebound due to glacial erosion within the Transantarctic Mountains. Geology 33, 221–224. https://doi.org/10.1130/G21068.1.
Vermeesch, P., 2010. HelioPlot, and the treatment of overdispersed (U-Th-Sm)/He data. Chem. Geol. 271, 108–111. https://doi.org/10.1016/j.chemgeo.2010.01.002.
Vermeesch, P., 2008. Three new ways to calculate average (U-Th)/He ages. Chem. Geol. 249, 339–347. https://doi.org/10.1016/j.chemgeo.2008.01.027.
Vermeesch, P., Seward, D., Latkoczy, C., Wipf, M., Günther, D., Baur, H., 2007. α-emitting mineral inclusions in apatite, their effect on (U-Th)/He ages, and how to reduce it. Geochim. Cosmochim. Acta 71, 1737–1746. https://doi.org/10.1016/j.gca.2006.09.020.
Welke, B., Licht, K., Hennessy, A., Hemming, S., Pierce Davis, E., Kassab, C., 2016. Applications of detrital geochronology and thermochronology from glacial deposits to the Paleozoic and Mesozoic thermal history of the Ross embayment, Antarctica. Geochem. Geophys. Geosyst. 17, 2762–2780. https://doi.org/10.1002/2015GC005941.
Whitehouse, P.L., Wiens, D.A., Gomez, N., King, M.A., 2019. Solid Earth change and the evolution of the Antarctic Ice Sheet. Nat. Commun., 1–14. https://doi.org/10.1038/s41467-018-08068-y.
Wilson, G.S., Pekar, S.F., Naish, T.R., Passchier, S., DeConto, R., 2008. Chapter 9 The Oligocene-Miocene boundary - Antarctic climate response to orbital forcing. Dev. Earth Environ. Sci. 8, 369–400. https://doi.org/10.1016/S1571-9197(08)00009-8.
Zachos, J.C., Dickens, G.R., Zeebe, R.E., 2008. An early Cenozoic perspective on greenhouse warming and carbon-cycle dynamics. Nature 451, 279–283. https://doi.org/10.1038/nature06588.
Zeitler, P.K., Enkelmann, E., Thomas, J.B., Watson, E.B., Ancuta, L.D., Idleman, B.D., 2017. Solubility and trapping of helium in apatite. Geochim. Cosmochim. Acta 209, 1–8. https://doi.org/10.1016/j.gca.2017.03.041.